



Noble gases in Paleozoic shale fluids document tectonic events and fluid migration in the Upper Yangtze Block

Rui Liu^{a,b,*}, Tao Wen^{c,**}, Daniele L. Pinti^d, Rui Xu^{a,b}, Fang Hao^e, Shang Xu^e, Zhiguo Shu^f

^a State Key Laboratory of Oil and Gas Reservoir Geology and Exploration (Southwest Petroleum University), Chengdu 610500, China

^b School of Geoscience and Technology, Southwest Petroleum University, Chengdu 610500, China

^c Department of Earth and Environmental Sciences, Syracuse University, Syracuse, New York 13244, United States

^d GEOTOP – Research Center on the dynamics of the Earth System, Université du Québec à Montréal, QC, Canada

^e School of Geosciences, China University of Petroleum, Qingdao 266580, China

^f SINOPEC Jianghan Oilfield Company, Qianjiang, Hubei 433124, China

ARTICLE INFO

Keywords:

Shale
Pore fluids
Noble gases
Fluid expulsion
Tectonic deformation
Yangtze Block

ABSTRACT

Major and noble gases of natural gas extracted from the low-permeability Paleozoic Wufeng-Longmaxi shale were measured to reconstruct the multi-stage, spatially varying tectonic evolution of the Upper Yangtze Block, China, one of the oldest parts of the Earth continents. The high gas dryness ratio [$C_1/(C_2 + C_3)$] and high carbon isotopic ratios ($\delta^{13}\text{C}-\text{C}_1$, $\delta^{13}\text{C}-\text{C}_2$, $\delta^{13}\text{C}-\text{CO}_2$) suggest a late mature thermogenic origin of shale gas. The highly fractionated atmospheric $^{20}\text{Ne}/^{36}\text{Ar}$ and $^{84}\text{Kr}/^{36}\text{Ar}$ ratios in our gas samples suggest they result from solubility-based partitioning of noble gases between oil and water followed by gas-water partitioning. Calculated volume ratios of oil, water, and gas phases vary spatially and temporally. In particular, the western Yangtze Block shows a lower reconstructed oil/water ratio, suggesting oil leakage promoted by the Triassic exhumation of Paleozoic shale, while a low gas/water ratio in the central-eastern Yangtze Block suggests gas leakage promoted by basin-wide Jurassic fold-thrust faulting. The lowest $\text{C}_1/^{36}\text{Ar}$ volume ratio around faults at the basin edges indicates extensive gas expulsion. Delineated radiogenic ^4He in gas samples are several orders lower than calculated in-situ produced radiogenic ^4He , likely suggesting widespread ^4He loss. Spatially-varying $^4\text{He}/\text{nucleogenic } ^{21}\text{Ne}$ ratios in the shale indicated that ^4He loss in the western Yangtze Block predated that in the central-eastern portion. Such He loss was also coupled with the Triassic exhumation and the Jurassic fold-thrust faulting episodes. In summary, noble gas in pore fluids extracted from low-permeability shale can preserve reliable records of tectonic events produced during upper crust evolution.

1. Introduction

Stable noble gases (He, Ne, Ar, Kr, Xe), which are chemically inert and present unique isotopic signatures for different sources (i.e., the atmosphere, the crust, and the mantle), have been proven to be a powerful tool to trace the movement and mixing of multi-phase pore fluids in shales that were not well documented by traditional geochemical tracers (Byrne et al., 2018; Györö et al., 2021; Wen et al., 2015; Wen et al., 2017).

Noble gases in shale pore fluids are mainly dominated by atmospheric and terrigenous (radiogenic or nucleogenic) sources. The atmospheric noble gases (ANG) are brought into deeper fluids along with the recharge of meteoric fluids (Air Saturated Water or ASW). ANG

elemental ratios (e.g., Ne/Ar, Kr/Ar, and Xe/Ar) in the ASW can be later modified (i.e., fractionated) by solubility-driven partitioning among multi-phase (water/oil/gas) fluids, e.g., hydrocarbons and water (Bosch and Mazor, 1988; Kharaka and Specht, 1988). Fractionated ANG elemental ratios thus generally record past complex fluid-rock interactions, which have been widely used to reconstruct the hydrodynamic system evolution during tectonic events or anthropogenic activities (Darrah et al., 2014; Wen et al., 2016). Terrigenous noble gases ($^4\text{He}^*$, $^{21}\text{Ne}^*$, and $^{40}\text{Ar}^*$, “*” denotes the radiogenic/nucleogenic component) are produced by nuclear reactions involving U, Th, and K decay or other light elements in rocks (Ballentine and Burnard, 2002). The production ratios in rocks, $^4\text{He}^*/^{40}\text{Ar}^*$, $^4\text{He}^*/^{21}\text{Ne}^*$, $^{21}\text{Ne}^*/^{40}\text{Ar}^*$, can be subsequently modified by the differentiated release of noble gases

* Corresponding author at: School of Geoscience and Technology, Southwest Petroleum University, Chengdu 610500, China.

** Corresponding author.

E-mail addresses: liurui@outlook.com (R. Liu), twen08@syr.edu (T. Wen).

into fluids, which depends on their closure temperatures in minerals, with He and Ne released at lower closure temperatures of 50–70 °C and Ar at temperatures of 230–300 °C (Ballentine et al., 1994; Snee, 2002). Metamorphic and volcanic events or tectonic deformation can further facilitate the thermal (Ballentine et al., 1994; Lowenstern et al., 2014; Mtili, 2021; Wen et al., 2018) or mechanical (Buttitta et al., 2020; Méjean et al., 2017) release of produced terrigenous noble gases (Kennedy et al., 2002; Pinti et al., 2011; Pinti and Marty, 1995). It is important to note that mantle-derived noble gases are mostly negligible or present in a trace amount in relatively shallow crustal fluids although they might be present in a larger amount in volcanic- or tectonically active regions (Byrne et al., 2020; Kennedy, and Soest, M.C.v., 2007; Zaputlyanova et al., 2019).

The Yangtze Block (also called Yangtze Craton or Yangtze Platform) is one of the oldest continental crust on Earth (Pearson et al., 2021). The breakthrough of shale gas exploration and production in the Paleozoic shales within the Yangtze Block in the last decades extracts massive crustal fluids from the deep-buried strata through industrial drillings, which provide valuable opportunities to study the geology and tectonic

history of the Yangtze Block. In this study, we measure noble gas signatures in shale gases that are collected from the Wufeng-Longmaxi shale (deposited during Late Ordovician-Early Silurian) within the Upper Yangtze Block in South China, to reconstruct the multi-stage, spatially varying tectonic evolution in the basin and its control on multi-phase subsurface fluids.

2. Geological settings

2.1. Regional tectonic deformation

The Yangtze Block, is one of the most complicated and largest Precambrian blocks in South China, surrounded by numerous fold-thrust belts (Fig. 1A). The origin of the Yangtze Block was allegedly related to the breakup of the Rodinia supercontinent (Wang et al., 2010). The persistent subduction of the Yangtze beneath the Cathaysia Block promoted the uplift of the Jiangnan-Xuefeng Orogen since ~1000 Ma ago (Wang et al., 2013) and the northward deepening of the Yangtze Shelf Sea during the Early Paleozoic (Zou et al., 2018). Abundant marine

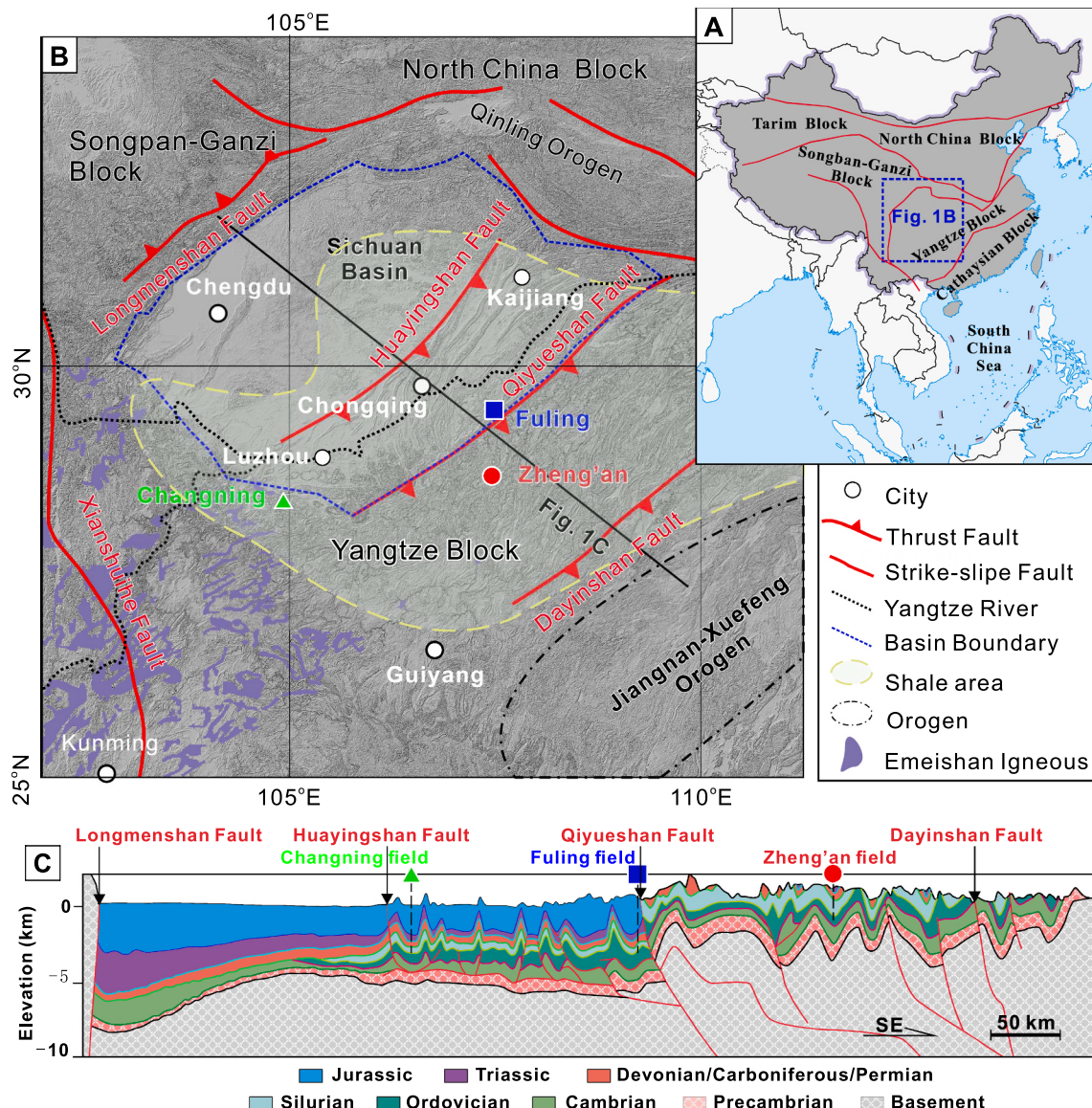


Fig. 1. (A) Location and tectonic setting of the Yangtze Block, (B) Fault system and the distribution of the organic-rich Paleozoic shale, i.e., the Wufeng-Longmaxi shale, in the Upper Yangtze Block. (C) A cross-section of the Upper Yangtze Block shows the distribution of sediments and deformation styles (Dong et al., 2015; Li et al., 2018; Liu et al., 2021b).

organic matter (dominated by plankton) was deposited and preserved in shales of the Upper Ordovician Wufeng Fm. and the Lower Silurian Longmaxi Fm. (i.e., Wufeng-Longmaxi shale) on the deep-water shelf (Hao and Zou, 2013; Liu et al., 2020a) (Fig. 1B). The Wufeng-Longmaxi shale has the estimate recoverable reserves of $>1.7 \times 10^{13} \text{ m}^3$, and can produce $>200 \times 10^8 \text{ m}^3$ of natural gas per year (Zou et al., 2021).

The Late Permian-Early Triassic collision of Indochina and the Yangtze Block along the Ailaoshan-Songma Suture triggered the uplift of the southwestern Yangtze Block. The Triassic collision between the Yangtze and the North China blocks generated the Qinling Orogen, subsequently followed by the collision between the Yangtze and the Songpan-Ganzi blocks along the Longmenshan Fault, which resulted in the exhumation of the southern and northeastern Sichuan Basin (Liu et al., 2021b). The Middle Triassic units were completely eroded in the Luzhou-Changning area of the Sichuan Basin. Whereas a flexural loading foredeep appeared in front of the Longmenshan Fault and was filled with a wedge-shaped package of terrestrial clastic rocks during the Late Triassic (Meng et al., 2005; Richardson et al., 2008). A northwest stepwise progression of deformation during the Middle Jurassic to Late Cretaceous generated a well-developed Mesozoic thrust system extending from the Jiangnan-Xuefeng Orogen to the Huayingshan Fault (Dong

et al., 2015; He et al., 2018; Li et al., 2018). The eastward extrusion of the Songpan-Ganzi Block during the Himalayan tectonic epoch resulted in uplift of the Sichuan Basin located on the western Yangtze Block. Particularly, the Qiyueshan Fault as the eastern boundary of the Sichuan Basin has undergone the most significant tectonic activation during the Late Eocene (Feng et al., 2023).

To better understand the spatial variation in tectonic deformation of the Upper Yangtze Block, three Paleozoic shale gas fields (i.e., the Changning, Fuling, and Zheng'an) located in different tectonic domains were selected for comparison in this study. As shown in the NE-SW cross-section of the Upper Yangtze Block (Fig. 1C), the tectonic deformation varies between the three sampling areas. The Triassic collision along the Longmenshan Fault on the West resulted in the forebulge and erosion in the Changning field (or along the line of Changning-Luzhou-Chongqing cities, Fig. 1B, C). The Jurassic fold-thrust deformation driven by the uplift of the Jiangnan-Xuefeng Orogen resulted in a more intensive exhumation in the Zheng'an field than the Changning field (Fig. 1C). Finally, the Fuling field is located in the vicinity of the Qiyueshan Fault, which is the eastern boundary of the Sichuan Basin, separating the thrust-fold system into thin- and thick-skinned thrust domains in the northwest and southeast, respectively (Fig. 1C). Because of the regional

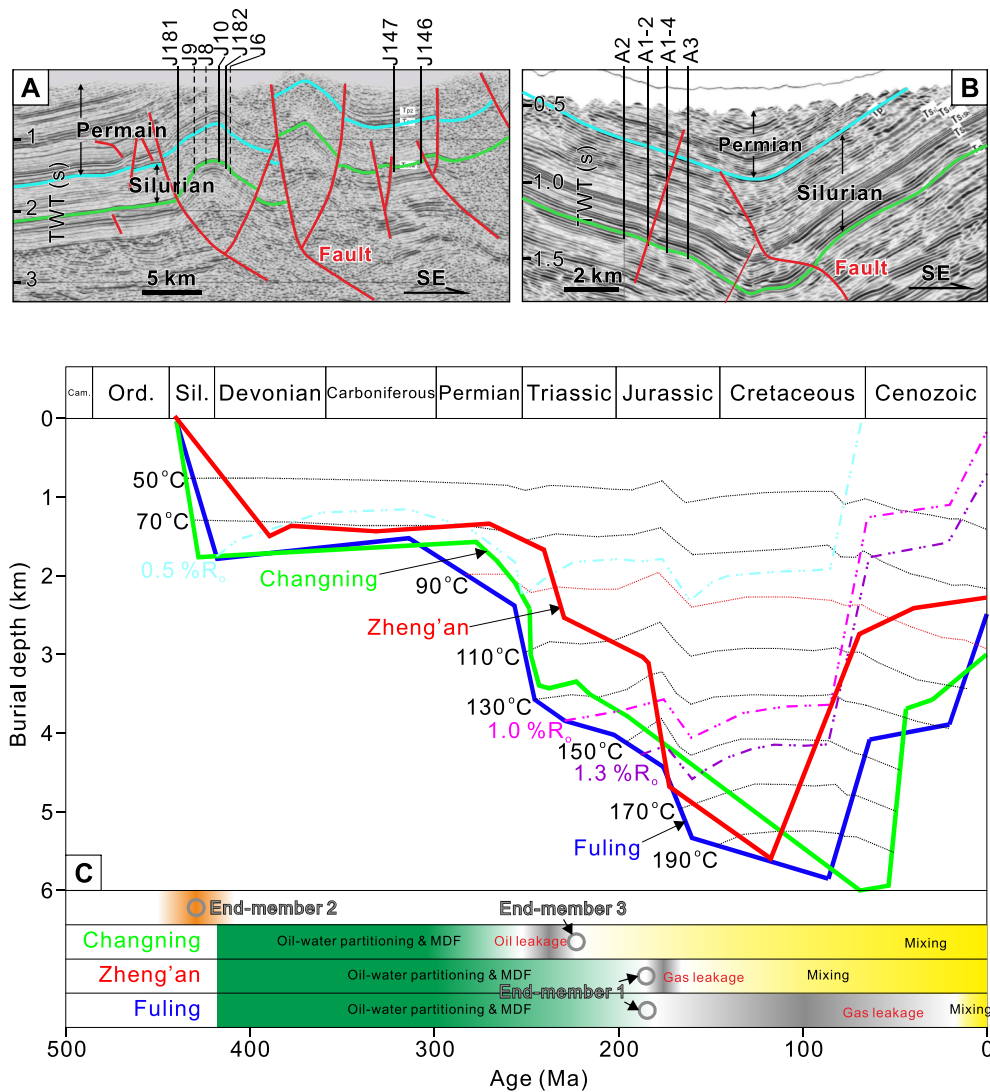


Fig. 2. Seismic reflection profiles of the (A) Fuling and (B) Zheng'an gas fields, respectively, show the faulting and deformation features. The well locations of gas samples were also projected. (C) Burial, thermal, and hydrocarbon generation histories of the Wufeng-Longmaxi shale in the Changning (Liu et al., 2021c), Fuling (Yang et al., 2017), and Zheng'an (Zhai et al., 2017) fields. Note that the tectonic exhumation occurred regionally during the Jurassic-Cretaceous, but only appeared in the Changning field during the Triassic. The End-members 1, 2, and 3 were established by section 4.2.2 and the timelines of section 5.5 were also shown.

variation in exhumation intensity, the fold-thrust structures widely appear along the Fuling field (Fig. 2A) but only syncline structures remained in the Zheng'an field (Fig. 2B). Additionally, in comparison to the Zheng'an field, faulting systems are more complex in the Fuling field due to the influence of the Qiyueshan Fault.

2.2. Hydrocarbon generation history

Thermal history simulations suggested that the Paleozoic Wufeng-Longmaxi shale acts as the source and the reservoir, starting to generate oil from plankton-rich kerogen before Early Permian. It reached the peak of oil generation during the Late Permian to Early Triassic, at a paleotemperature of approximately 120 °C (Liu et al., 2021c; Yang et al., 2017; Zhai et al., 2017) (Fig. 2C). After the regionally heterogeneous tectonic deformation of Late Triassic (particularly in the Changning field), the Wufeng-Longmaxi shale was buried to the depth of 5 to 6 km, corresponding to a maximum paleotemperature of approximately 200 °C (Fig. 2C). Because of the high temperature, the oil retained in the organic or inorganic pore system of the Wufeng-Longmaxi shale was completely cracked into gaseous hydrocarbons with low molecular weight (Dai et al., 2016; Hao and Zou, 2013). The Late Jurassic uplift of the Jiangnan-Xuefeng Orogen promoted the gradual exhumation and cooling of the Wufeng-Longmaxi shale. The current burial depth of the Wufeng-Longmaxi shale in the Changning, Fuling, and Zheng'an fields varies from 2 to 3 km, corresponding to an average reservoir temperature of 100 °C. The gravity separation of multiphase fluids in organic-rich shale is not significant because of its low permeability, and thus no remarkable hydrocarbon-water interface following the hydrocarbon (oil or gas) generation. Nevertheless, water and hydrocarbon phases coexist in micro or nano pores of the shale gas system as indicated by the water saturation of more than 20–30 % (Liu et al., 2020a).

3. Sampling and analytical methods

In November 2020, 24 gas samples were collected from 12 production wells in the Fuling ($n = 8$; Sample ID starts with a 'J') and Zheng'an ($n = 4$; Sample ID starts with an 'A') shale gas fields which both target the Wufeng-Longmaxi shale (Fig. 2B; Table S1). Natural gases were directly collected from the wellhead using a manifold to reduce the pressure (usually ≤ 50 bars) before flowing the gas into IsoTube at 3 bars maximum. Air contamination during sampling was minimized by allowing the gas to flush through the system for at least 10 min before shutting off the valve connecting the IsoTube to the wellhead.

At each well, one IsoTube sample was analyzed for major gas composition [i.e., methane (C₁), ethane (C₂), propane (C₃), N₂, O₂, CO₂] at the State Key Laboratory of Oil and Gas Reservoir Geology and Exploration at the Southwest Petroleum University, using a Shimadzu 2010 Gas Chromatograph. Carbon isotopes of methane ($\delta^{13}\text{C-C}_1$), ethane ($\delta^{13}\text{C-C}_2$), and carbon dioxide ($\delta^{13}\text{C-CO}_2$) were analyzed using an HP6890 GC interfaced to a Thermo Scientific® Delta V Plus (Table S1). The $\delta^{13}\text{C}$ values are given relative to the PDB (Pee Dee Belemnite) standard (Craig, 1957) with an $\pm 2\sigma$ error of 0.5 ‰.

The other set of samples were shipped to and analyzed at the Noble Gas Laboratory of the University of Michigan for the complete set of stable noble gases (He, Ne, Ar, Kr, Xe) within approximately two weeks after the sample collection to minimize air contamination (Tables S2 and S3). Collected gas samples were transferred from the IsoTube to a copper tube, which was then attached to a vacuum extraction and purification system (Liu et al., 2021a). After purification on Ti sponge and Cu/CuO getters, He and Ne were analyzed using a Thermo® Helix SFT mass spectrometer while Ar, Kr, and Xe were sequentially inlet into a Thermo® ARGUS VI mass spectrometer using a Janis® computer-controlled double-head cryo-separator. Detailed steps of extraction, purification, and analysis procedures are described by Wen et al. (2016, 2017, 2018) and Pinti et al. (2017). Standard errors ($\pm 1\sigma$) for volume

fractions are 1.5, 1.3, 1.3, 1.5, and 2.2 % for He, Ne, Ar, Kr, and Xe, respectively (Tables S2 and S3). Data for shale gas samples collected from the Changning field (Sample ID starts with an 'H' or an 'N'), which also targets the Wufeng-Longmaxi shale, were reported by Liu et al. (2021a) and compiled here for comparison.

4. Results

4.1. Major gas composition and carbon isotopes

Most gas samples consist of ~98 % of hydrocarbons with gas dryness ratios [i.e., C₁/(C₂ + C₃)] varying from 133.7 to 235.7, except for sample J181 (93 %) (Table S1). Higher concentrations of O₂, CO₂, and N₂ and lower wellhead pressure of 1–2 bars in J181 well (Table S1) suggest atmospheric contamination. Except for sample J181, $\delta^{13}\text{C-C}_1$, $\delta^{13}\text{C-C}_2$, and $\delta^{13}\text{C-CO}_2$ of the Fuling gas samples range from -32.2 to -30.2 ‰, -36.6 to -34.3 ‰, and 0.6 to 5.1 ‰, respectively. For Zheng'an gas samples, $\delta^{13}\text{C-C}_1$, $\delta^{13}\text{C-C}_2$, and $\delta^{13}\text{C-CO}_2$ vary from -35.9 to -34.6 ‰, -38.5 to -38.3 ‰, and -5.3 to -3.8 ‰, respectively. The gas dryness ratio and carbon isotopes ($\delta^{13}\text{C-C}_1$, $\delta^{13}\text{C-C}_2$, $\delta^{13}\text{C-CO}_2$) of most samples are generally consistent with the previously reported values from the Wufeng-Longmaxi shale, suggesting a late mature thermogenic origin of hydrocarbons and CO₂ (Feng et al., 2022; Liu et al., 2021a; Milkov et al., 2020) (Fig. 3). Compared to the Fuling samples, Zheng'an samples generally show lower gas dryness ratio of <175 and isotope ratios ($\delta^{13}\text{C-C}_1 < -34$ ‰, $\delta^{13}\text{C-C}_2 < -38$ ‰, and $\delta^{13}\text{C-CO}_2 < -3$ ‰) indicating a lower thermal maturity level.

4.2. Noble gases

4.2.1. Helium

The ^4He concentration of most gas samples varies between $(1.40 \pm 0.02) \times 10^{-4}$ and $(4.16 \pm 0.06) \times 10^{-4} \text{ cm}^3 \text{ STP/cm}^3$, which is higher than the atmospheric value of $(5.24 \pm 0.05) \times 10^{-6} \text{ cm}^3 \text{ STP/cm}^3$ (Ozima and Podosek, 2002). Measured $^3\text{He}/^4\text{He}$ ratios range from $(0.0087 \pm 0.0003)\text{R}_\text{A}$ to $(0.183 \pm 0.006)\text{R}_\text{A}$ [R_A refers to the atmospheric ratio of $1.384 \pm 0.013 \times 10^{-6}$ (Clarke et al., 1976)], which are similar to the typical crustal $^3\text{He}/^4\text{He}$ value of $\sim 0.01\text{R}_\text{A}$ or slightly higher (Ballentine and Burnard, 2002; Oxburgh et al., 1986) suggesting a dominant crustal origin for helium (Table S2, Fig. 4). Sample J181 has a $^3\text{He}/^4\text{He}$ ratio of $(1.15 \pm 0.03)\text{R}_\text{A}$ which approaches the atmospheric value, together with air-like ^4He amount of $(0.05 \pm 0.01) \times 10^{-4} \text{ cm}^3 \text{ STP/cm}^3$ confirming that the sample J181 is air contaminated (Table S3). This sample thus will not be included in the following discussion.

4.2.2. Neon

The ^{20}Ne concentration of most samples ranges between $(2.40 \pm 0.03) \times 10^{-8}$ and $(4.13 \pm 0.05) \times 10^{-6} \text{ cm}^3 \text{ STP/cm}^3$, lower than the atmospheric value of $(1.645 \pm 0.004) \times 10^{-5}$ except for the air-contaminated sample J181 (Eberhardt et al., 1965; Ozima and Podosek, 2002) (Table S3). The relatively low $^4\text{He}/^{20}\text{Ne}$ ratios suggest air contamination to some extent in samples J6 and J8 (Fig. 4). The $^{20}\text{Ne}/^{22}\text{Ne}$ ratio of Fuling and Zheng'an gas samples ranges from (9.79 ± 0.01) to (10.302 ± 0.003) , mostly exceeding the atmospheric value of 9.80 (Eberhardt et al., 1965). This is likely related to mass-dependent fractionation rather than the contribution of mantle Ne as detailed in the following sections (Fig. 5). The $^{21}\text{Ne}/^{22}\text{Ne}$ ratios range from the atmospheric value of 0.0290 (J6, J8, and J181) to 0.0418 pointing to the addition of nucleogenic $^{21}\text{Ne}^*$ in some samples (Fig. 5). The Ne isotopes of Zheng'an and Fuling samples (except J182, which shows an exceptionally high degree of fractionation) generally follow the predicted trend of mass-dependent fractionation (MDF, Eqs. 1 to 3 of Text S1) and air-crust mixing. This trend suggests the binary mixing of two end-members: fractionated air ($^{21}\text{Ne}/^{22}\text{Ne} = 0.0295$, $^{20}\text{Ne}/^{22}\text{Ne} = 10.18$) and nucleogenic component ($^{21}\text{Ne}/^{22}\text{Ne} = 0.05$, $^{20}\text{Ne}/^{22}\text{Ne} = 9.35$)

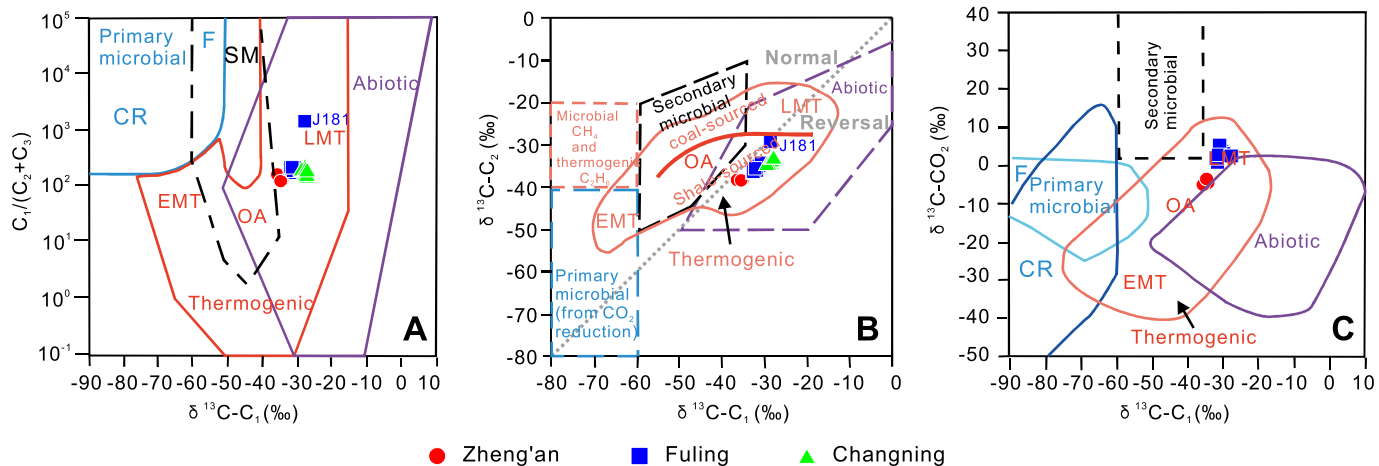


Fig. 3. Gas samples were plotted on the gas genetic diagrams of Milkov et al. (2020). Abbreviations: CR – CO_2 reduction, F – methyl-type fermentation, SM – secondary microbial, EMT – early mature thermogenic gas, OA – oil-associated (mid-mature) thermogenic gas, LMT – late mature thermogenic gas. Hydrocarbons and CO_2 in gas samples obtained from the Wufeng-Longmaxi shale are dominant by a late-mature thermogenic origin.

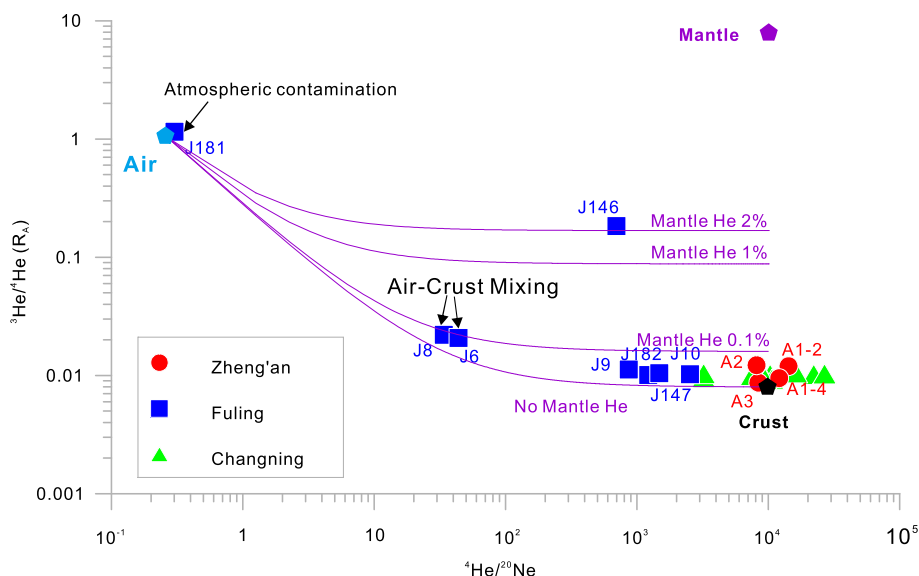


Fig. 4. ${}^3He/{}^4He$ versus ${}^4He/{}^{20}Ne$ ratios for Paleozoic shale gas samples of the Upper Yangtze Block. The purple lines represent the mixing of air- and crust-derived noble gases, and air- and mantle-derived noble gases. ${}^3He/{}^4He$ and ${}^4He/{}^{20}Ne$ ratios of air, crust, and mantle endmembers are $1R_A [R_A = (1.384 \pm 0.006) \times 10^{-6}]$ and 0.274 (Ozima and Podosek, 2002), 0.01R_A and 10,000, 8R_A and 10,000 (Ballentine and Burnard, 2002; Graham, 2002; Oxburgh et al., 1986), respectively (for more details please see Table S4). Except for the slight influence of mantle fluid on sample J146, other samples are dominated by the binary mixing between air and crustal fluids. Particularly, the samples J181, J8, and J6 were air contaminated. (For interpretation of the references to colour in this figure legend, the reader is referred to the web version of this article.)

(Fig. 5).

4.2.3. Argon, krypton, and xenon

The ${}^{36}Ar$ concentration varies between $(6.1 \pm 0.1) \times 10^{-8}$ and $(5.48 \pm 0.07) \times 10^{-6} \text{ cm}^3 \text{ STP/cm}^3$, lower than the atmospheric value of $(3.142 \pm 0.003) \times 10^{-5} \text{ cm}^3 \text{ STP/cm}^3$ (Mark et al., 2011) (except air-contaminated sample J181), with Fuling gas samples generally reporting higher values than Zheng'an gas samples (Table S3). The ${}^{38}Ar/{}^{36}Ar$ ratio ranges from (0.1842 ± 0.0003) , lower than the atmospheric value of 0.1880 (Ozima and Podosek, 2002), up to (0.1889 ± 0.0009) (Table S2). The deviation of ${}^{38}Ar/{}^{36}Ar$ and ${}^{20}Ne/{}^{22}Ne$ ratios of the Fuling and Zheng'an gas samples from corresponding air values are also consistent with MDF deviating from the air values (Fig. 6A), based on which we can rule out the presence of mantle Ne. The ${}^{40}Ar/{}^{36}Ar$ ratios range from the atmospheric value of 298.6 ± 0.3 (Lee et al., 2006; Mark et al., 2011) (J6, J8) to 875 ± 2 (Table S2, Fig. 6B), indicating the

addition of terrigenous (i.e., crustal) ${}^{40}Ar^*$. Similar to the ${}^{21}Ne/{}^{22}Ne$ ratio, the ${}^{40}Ar/{}^{36}Ar$ ratio of Zheng'an samples is higher than that of Fuling samples. Krypton and xenon isotopic ratios are mainly atmospheric within uncertainties (Table S2) or slightly mass-dependent fractionated and will not be discussed further.

5. Discussion

5.1. Gas generation

Unlike most hydrocarbon samples where $\delta^{13}C$ value in alkanes usually increases with the carbon number (Lorant et al., 1998), Fuling and Zheng'an gas samples show an “isotopic reversal” pattern i.e., $\delta^{13}C - C_1 > \delta^{13}C - C_2$ as also previously observed in the Wufeng-Longmaxi samples (Dai et al., 2016; Feng et al., 2022) (Fig. S1A). The mixing of gases generated by the secondary cracking of retained oil (or wet gas) at

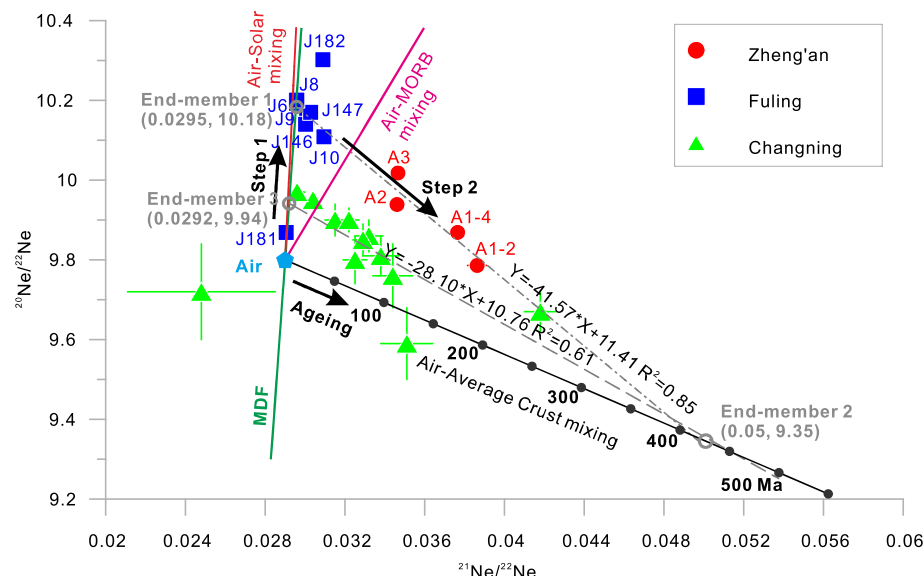


Fig. 5. Cross plots of $^{20}\text{Ne}/^{22}\text{Ne}$ with $^{21}\text{Ne}/^{22}\text{Ne}$ for the Paleozoic shale gas samples of the Upper Yangtze Block. Typical mixing lines of air-crust and air-mantle (mantle Ne is assumed to be sourced from the Mid-Ocean Ridge Basalt or MORB) are also shown as following Castro et al. (2009) (Please see Table S4 for more details). Predicted ratios by following the mass-dependent fractionation (MDF, S1) are also shown for comparison. Each regression line represents a mixing of an MDF fractionated air endmember and a crust endmember. Corresponding air values are indicated (Györe et al., 2024; Györe et al., 2019; Mark et al., 2011; Ozima and Podosek, 2002). The age points on the air-crust line were estimated by Eq. 16 of Text S6.

elevated maturity was suggested to be the key mechanism producing the carbon isotopic reversal in the Paleozoic Wufeng-Longmaxi shale (Hao and Zou, 2013) (Fig. S1A). The secondary cracking process in the Wufeng-Longmaxi shale is evident based on the decoupled C_1/C_2 and C_2/C_3 ratios, i.e., unvaried C_1/C_2 ratio with highly variable C_2/C_3 ratios (Fig. S1B). The physical experiments conducted by Prinzhofen and Huc (1995) revealed that: the C_2/C_3 ratio almost keeps unchanged during primary cracking of kerogen but increases dramatically during the secondary cracking; whereas, the C_1/C_2 ratio is elevated gradually during primary cracking but almost constant during secondary cracking (Fig. S1C). The cracking of oil can produce ^{12}C -rich ethane and result in the decreasing of $\delta^{13}\text{C}-\text{C}_2$ (Fig. S1A); then the further elevated thermal maturity level may contribute to the cracking of wet gas, and the preferential break of weaker ^{12}C bonds can induce the increasing of $\delta^{13}\text{C}-\text{C}_2$ (Fig. S1A) (Hao and Zou, 2013).

5.2. ANG elemental fractionation in multiphase fluids

The $^{20}\text{Ne}/^{36}\text{Ar}$ ratios of Fuling and Zheng'an gas samples range from 0.56 to 0.91 and 0.39 to 0.46, respectively (Table S3). All samples exceed the expected $^{20}\text{Ne}/^{36}\text{Ar}$ value of 0.16–0.18 in the ASW (Smith and Kennedy, 1983), while Fuling samples even exceed the corresponding air value of 0.52 (Ozima and Podosek, 2002). To exclude the influence of MDF on $^{20}\text{Ne}/^{36}\text{Ar}$ values (Figs. 5, 7A), the MDF-altered $^{20}\text{Ne}/^{36}\text{Ar}$ ratios (denoted as $^{20}\text{Ne}_{\text{air-fra}}/^{36}\text{Ar}$) of Fuling and Zheng'an gas samples can be calculated by following Ballentine and O'Nions (1992) (Text S2). Calculated $^{20}\text{Ne}_{\text{air-fra}}/^{36}\text{Ar}$ ratios of Fuling and Zheng'an gas samples show a wider range from 0.20 to 1.25 (except for air-contaminated samples J181, J8, and J6) (Table S3, Fig. 7B), suggesting that other fractionation mechanism(s) in addition to MDF should also be considered.

Fluid degassing can also cause noble gas fractionation due to the different solubilities of light vs. heavy noble gases (Ballentine et al., 1991). However, a single-stage fractionation model, which simply considers the ASW degassing and can only yield a maximum $^{20}\text{Ne}_{\text{air-fra}}/^{36}\text{Ar}$ ratio of air value, is not sufficient for explaining the wide range of $^{20}\text{Ne}_{\text{air-fra}}/^{36}\text{Ar}$ ratio in our samples (Fig. 7B). Other more complex multi-phase fractionation models were previously proposed to explain

elevated $^{20}\text{Ne}/^{36}\text{Ar}$ ratio, e.g., two-stage groundwater gas stripping and redissolution (GGSR) fractionation (Gilfillan et al., 2008), and two-stage oil-modified groundwater-exsolution (OMGE) fractionation (Wen et al., 2017; Zhou et al., 2012). The GGSR model suggests that gas stripped from the groundwater then re-dissolve into groundwater due to the fluctuations of reservoir temperature or pressure, which can enhance the dissolution of heavier noble gases (e.g., ^{36}Ar) because the noble gas solubility in water positively correlates with atomic mass (Weiss, 1971a; Weiss, 1971b); thus, $^{20}\text{Ne}/^{36}\text{Ar}$ ratio in the residual gas phase will dramatically increase. Noble gas is much more soluble in crude oil than in water (Kharaka and Specht, 1988), and heavier noble gases are more soluble than light ones in oil. Following the OMGE model, a water phase is first in contact with an oil phase (i.e., first stage) leading to the preferential stripping of heavier noble gases from water to oil. Therefore, the residual water phase will show a higher $^{20}\text{Ne}/^{36}\text{Ar}$ ratio compared to ASW conditions but lower $^{84}\text{Kr}/^{36}\text{Ar}$ (or $^{132}\text{Xe}/^{36}\text{Ar}$) ratios. The residual water phase is then in contact with a natural gas phase (i.e., second stage) causing further relative enrichment in lighter noble gases (e.g., ^{20}Ne) but relative depletion in heavier noble gases (e.g., ^{84}Kr or ^{132}Xe) in the gas phase, similar to the single-stage fractionation or even GGSR models (Smith and Kennedy, 1983).

The oil phase should be considered in the fractionation model as the Wufeng-Longmaxi shale once generated oil (Dai et al., 2016; Liu et al., 2021a) (Fig. 2C). Therefore, the OMGE model, as the more viable option, is further explored below to explain observed $^{20}\text{Ne}_{\text{air-fra}}/^{36}\text{Ar}$ ratios in our gas samples. The OMGE model procedures are described by Eqs. 7 and 8 of Text S3 with the first stage (i.e., oil-water interaction) occurring at a paleo reservoir temperature of $\sim 120^\circ\text{C}$ when massive oil (assuming a general oil density of 0.8 g/cm^3) is generated in the Paleozoic Wufeng-Longmaxi shale. The second stage (gas-water interaction) is assumed to take place at the current average reservoir temperature of $\sim 100^\circ\text{C}$ ($80\text{--}120^\circ\text{C}$) (Fig. 2C). As shown in Fig. 7B, OMGE results are generally consistent with estimated $^{20}\text{Ne}_{\text{air-fra}}/^{36}\text{Ar}$ and $^{84}\text{Kr}/^{36}\text{Ar}$ ratios of the gas samples when assuming an initial ASW noble gas composition at 20°C .

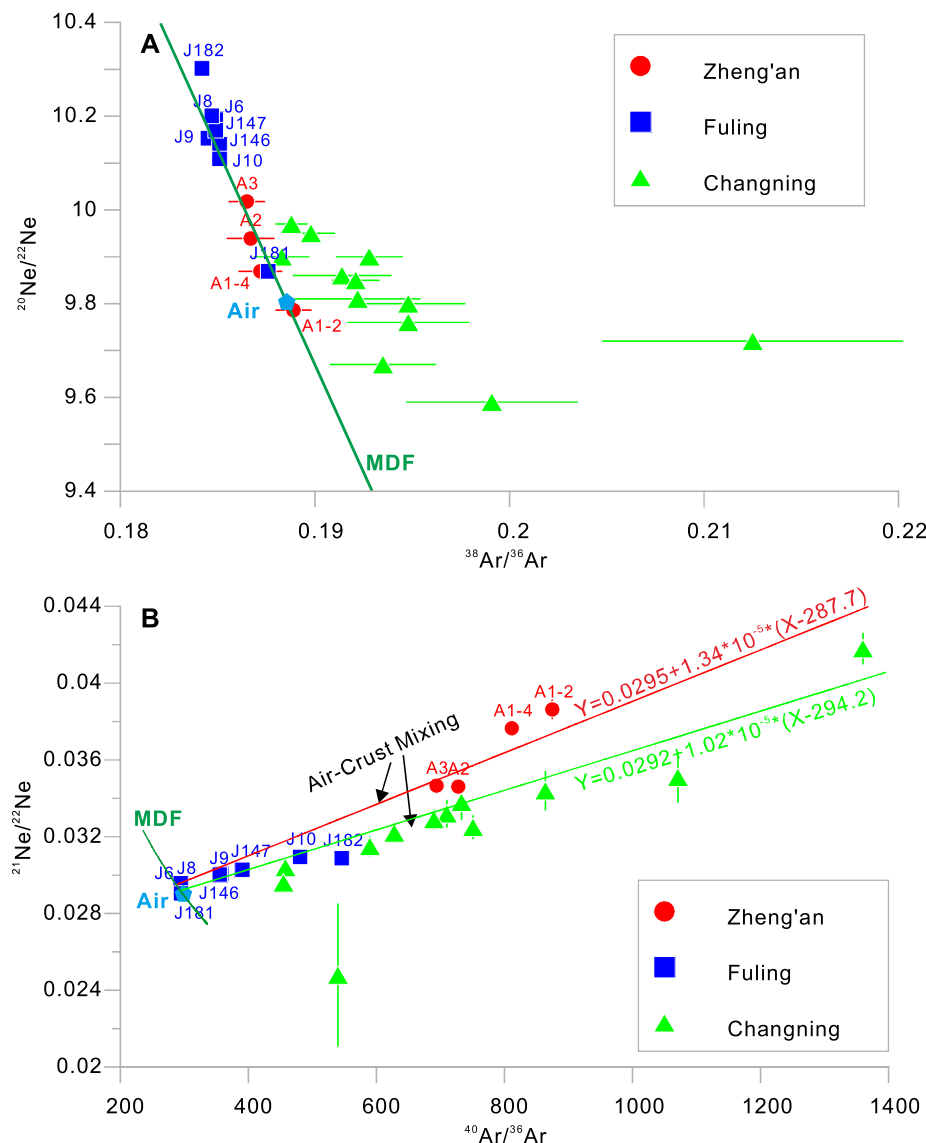


Fig. 6. Cross plots of (A) $^{20}\text{Ne}/^{22}\text{Ne}$ with $^{38}\text{Ar}/^{36}\text{Ar}$ and (B) $^{21}\text{Ne}/^{22}\text{Ne}$ with $^{40}\text{Ar}/^{36}\text{Ar}$ ratios for the Paleozoic shale gas samples of the Upper Yangtze Block. Predicted ratios by following the mass-dependent fractionation (MDF, Text S1) are also shown for comparison. Corresponding air values are indicated (Györe et al., 2024; Györe et al., 2019; Mark et al., 2011; Ozima and Podosek, 2002) (Please see Table S4 for more details). The $^{20}\text{Ne}/^{22}\text{Ne}$ and $^{38}\text{Ar}/^{36}\text{Ar}$ ratios of Fuling and Zhang'an samples generally align with the MDF line in Fig. 6A, excluding the influence of mantle fluids on the $^{20}\text{Ne}/^{22}\text{Ne}$ ratio. Each regression line of Fig. 6B represents a mixing of an MDF fractionated air endmember and a crust endmember. Corresponding air values are indicated and derived from the literature (Györe et al., 2019; Mark et al., 2011).

5.3. Fluid volumes estimation

Measured ANG elemental and isotopic ratios not only document the multi-stage, multi-phase interaction but also help quantify the volumetric ratios (i.e., $V_{\text{oil}}/V_{\text{water}}$ and $V_{\text{gas}}/V_{\text{water}}$) of oil, water, and gas phases involved in the fractionation processes. The complete cracking of oil to gas would not affect noble gas isotopes (e.g., $^{20}\text{Ne}/^{36}\text{Ar}$) of the hydrocarbon phase, but would decrease concentrations as the hydrocarbon phase expanded (e.g., Byrne et al. (2018)). Instead, the change of volume ratio of hydrocarbon to water or gas to oil in the open system, can alter the solubility equilibrium of hydrocarbon-water, oil-gas phases, and change the isotope ratios. These volumetric ratios for gas samples of the Wufeng-Longmaxi shale can be estimated based on the OMGE model using Eqs. 9 and 10 of Text S3.

Calculated $V_{\text{oil}}/V_{\text{water}}$ ratios in the pore system of the Wufeng-Longmaxi shale in the Fuling and Zheng'an fields are similar (~ 0.25), both of which are higher than that of the Changning field (~ 0.02).

(Table S5). This likely suggests less oil was present in the Changning field than in the other two fields, which argues against the higher total organic carbon (TOC) content (i.e., more oil and higher $V_{\text{oil}}/V_{\text{water}}$ ratio) in the Changning field (Liu et al., 2020a; Liu et al., 2020b). As shown in Fig. 2C, the peak of oil generation ($\text{Ro} = \sim 1.0\%$) appeared during Triassic, suggesting that the oil-water ratio would gradually increase to a maximum value during Triassic, i.e., the critical oil-water ratio mainly appeared during Triassic. It is essential to point out that the Triassic oil generation in the Wufeng-Longmaxi shale (Gao et al., 2017; Liu et al., 2020c) almost synchronized with the intense deformation of the western Yangtze Block (Meng et al., 2005; Richardson et al., 2008; Wang et al., 2013) (Fig. 2C). In particular, the Changning area was exhumed (Liu et al., 2021b), which might lead to the massive oil leakage from the pore system of the Wufeng-Longmaxi shale in the Channing field. During the rapid exhumation, the Wufeng-Longmaxi shale can become overpressured relative to adjacent carrier beds that have equilibrated more rapidly to the new hydrostatic conditions. This pressure gradient

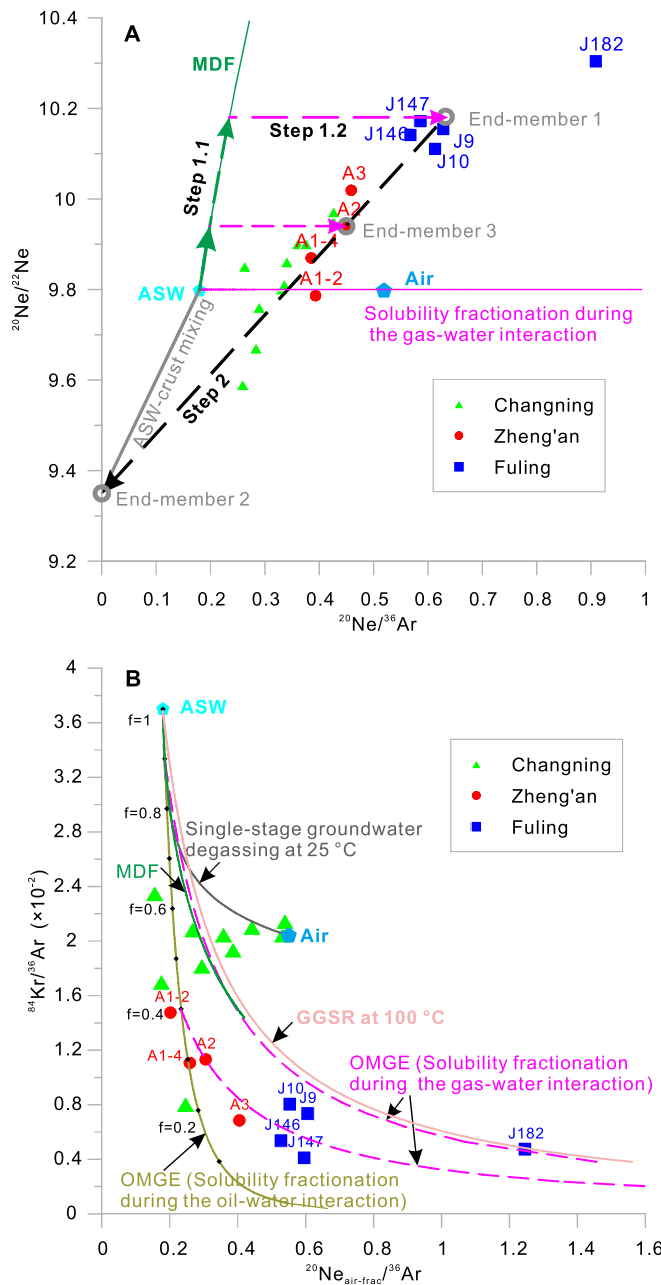


Fig. 7. Cross plots of (A) $^{20}\text{Ne}/^{22}\text{Ne}$ versus $^{20}\text{Ne}/^{36}\text{Ar}$ ratios and (B) $^{84}\text{Kr}/^{36}\text{Ar}$ versus $^{20}\text{Ne}_{\text{air-frac}}/^{36}\text{Ar}$ ratios of shale gas dasamples obtained from the Upper Yangtze Block. End-members 1, 2, and 3 in Fig. 8A were sourced from Fig. 5. $^{20}\text{Ne}_{\text{air-frac}}$ in Fig. 8B was estimated by SI S2. Predicted values in the gas phase following an oil-modified groundwater exsolution (OMGE, SI S3) model under oil-water distillation at 120 °C and gas-water distillation at 100 °C. Calculated values in the gas phase following the mass-dependent fractionation (MDF), the single-stage groundwater degassing model for an open system under 25 °C, and the groundwater gas stripping and re-dissolution (GGSR) model at 100 °C also shown. The $^{20}\text{Ne}/^{36}\text{Ar}$ and $^{84}\text{Kr}/^{36}\text{Ar}$, ratios of the gas samples are best explained by the OMGE fractionation model.

between the shale and carrier beds would trigger intense oil expulsion. This oil expulsion process was suggested to be the primary migration of the conventional petroleum systems in the Permian reservoirs of the area (Yang et al., 2021). Therefore, the relatively lower $V_{\text{oil}}/V_{\text{water}}$ ratio in the Changning field than the other two fields suggests more extensive oil expulsion from the pore system of Wufeng-Longmaxi shale in the Changning area.

The majority of gas in the Paleozoic Wufeng-Longmaxi shale was

generated by in-situ thermal cracking of oil (Dai et al., 2016; Liu et al., 2021a). As shown in Fig. 2C, the gas generation after $\text{Ro} = \sim 1.0\text{--}1.2\%$ would increase the gas-water ratio with burial depth or temperature increases until the Jurassic tectonic uplift. Despite the higher $V_{\text{oil}}/V_{\text{water}}$ ratio, gas samples from the Fuling and Zheng'an fields generally yield lower $V_{\text{gas}}/V_{\text{oil}}$ ratios than Changning samples. In other words, a larger oil volume did not yield a larger hydrocarbon gas volume in the pore system of the Wufeng-Longmaxi shale from the Fuling and Zheng'an fields. The observed slight variability in gas thermal maturity from these three gas fields (Figs. 3, S1) can serve as one possible explanation for the different $V_{\text{oil}}/V_{\text{water}}$ and $V_{\text{gas}}/V_{\text{oil}}$ ratios calculated for these three fields. Another viable mechanism to account for various $V_{\text{gas}}/V_{\text{oil}}$ ratios from field to field is that gas expulsion following the massive gas generation has occurred among these three gas fields. Since Jurassic, the uplift of the Jiangnan-Xuefeng Orogen resulted in the compression and exhumation of the Paleozoic Wufeng-Longmaxi shale from the southeast to the northwest (He et al., 2018; Wang et al., 2013), which can trigger more intense fold-thrust deformation in the central Yangtze Block (e.g., Zheng'an and Fuling areas) relative to the western Yangtze Block (e.g., Changning area) (Figs. 1B, C, 2C). The complex faulting system and thinning of overlying formations (Fig. 1C) would promote the massive gas expulsion and decrease the $V_{\text{gas}}/V_{\text{oil}}$ ratio in the pore system of the Wufeng-Longmaxi shale in the Fuling and Zheng'an areas.

5.4. Episodic crustal noble gas loss

Helium contents in most Changning, Fuling, and Zheng'an samples are dominated by radiogenic $^4\text{He}^*$ (Eq. 11 of Text S4), except for J146 which might show a trivial contribution of mantle He (approximately 2 %) and air-contaminated J181, J8, J6 (Fig. 4). Crustal He can be produced either in-situ within the shale or externally from deeper formations (Cheng et al., 2023; Cheng et al., 2021). The in-situ produced ^4He [i.e., $(^4\text{He}_{\text{in-situ}})_{\text{gas}}$] calculated by Eqs. 13 to 15 of Text S5 would be (0.00163–0.0057), (0.011–0.0394), and (0.00314–0.00705) cm³ STP/cm³ for Changning, Fuling, and Zheng'an samples, respectively, which are several orders higher than measured ^4He values (Table S3), suggesting that extensive episodic $^4\text{He}^*$ loss from the Paleozoic Wufeng-Longmaxi shale might have occurred in the Upper Yangtze Block.

The release of radiogenic (or nucleogenic) $^4\text{He}^*$, $^{21}\text{Ne}^*$, and $^{40}\text{Ar}^*$ from minerals into fluids is temperature-dependent (Ballentine et al., 2002; Hunt et al., 2012; Moore et al., 2018). Due to different atomic radii, $^4\text{He}^*$, $^{21}\text{Ne}^*$, and $^{40}\text{Ar}^*$ are sequentially released from the rock with increasing closure temperatures. As the temperature increases, $^4\text{He}^*/^{21}\text{Ne}^*$ and $^4\text{He}^*/^{40}\text{Ar}^*$ ratios would decrease and progressively approach the predicted crustal $^4\text{He}^*/^{21}\text{Ne}^*$ or $^4\text{He}^*/^{40}\text{Ar}^*$ ratios dependent on U, Th, K contents of the host shale. The elevated $\delta^{13}\text{C-C}_1$, $\delta^{13}\text{C-C}_2$, and $\text{Ln}(\text{C}_1/\text{C}_2)$ in Fig. S1 suggest that the thermal maturity of the Wufeng-Longmaxi shale was generally higher than that of the North American shales. Therefore, $^4\text{He}^*/^{21}\text{Ne}^*$ or $^4\text{He}^*/^{40}\text{Ar}^*$ ratios in the Wufeng-Longmaxi shale of the Upper Yangtze Block are predicted to be lower (due to more release of heavy noble gases) than North American shales if they originated from source rocks with similar chemical composition (Fig. 8A). This prediction holds true for most North American shales, e.g., Eagle Ford shale (Byrne et al., 2018), Haynesville shale (Byrne et al., 2020), Marcellus shale (Hunt et al., 2012), and Barnett shale (Wen et al., 2017). The exception is Antrim shale in Michigan (U.S.) which shows extremely low $^4\text{He}/^{21}\text{Ne}$ or $^4\text{He}/^{40}\text{Ar}$ ratios (after correction for air component), as caused by the injection of mantle ^{21}Ne and ^{40}Ar (Wen et al., 2015).

Calculated $^4\text{He}^*/^{40}\text{Ar}^*$ ratios of Fuling, Zheng'an, and Changning samples are generally around 5 to 9 (Fig. 8A), which is lower than the predicted ratio of ~ 25 and 15–17 assuming a total release of $^{40}\text{Ar}^*$ from the Wufeng-Longmaxi shale (Liu et al., 2021a) or the general organic-rich shales (Hunt et al., 2012) respectively (considering the low K/U ratio of organic-rich shale relative to the average crustal composition (Hunt et al., 2012)). The maximum reservoir temperature (~ 200 °C) in

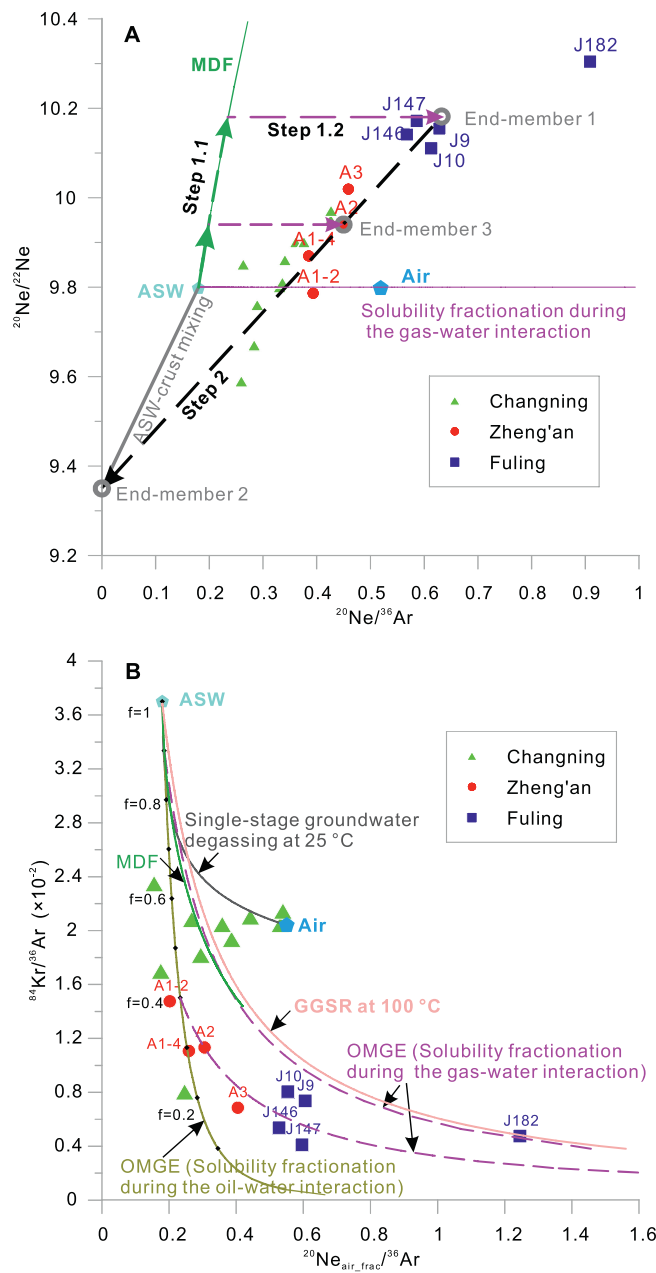


Fig. 8. Cross plots of (A) $^{4}\text{He}^*/^{40}\text{Ar}^*$ versus $^{4}\text{He}^*/^{21}\text{Ne}^*$ ratios, (B) $^{4}\text{He}^*/^{40}\text{Ar}^*$ versus $^{84}\text{Kr}^*/^{36}\text{Ar}^*$ ratios, and (C) $^{21}\text{Ne}^*/^{40}\text{Ar}^*$ versus $^{4}\text{He}^*/^{21}\text{Ne}^*$ ratios of the gas samples obtained from the Paleozoic shale of the Upper Yangtze Block. Samples of North American shales (Marcellus (Hunt et al., 2012), Barnett (Wen et al., 2017), Eagle Ford (Byrne et al., 2018), Haynesville (Byrne et al., 2020), Antrim (Wen et al., 2015)) were added in Fig. 9A for comparison. Corresponding average organic-rich black shales and Wufeng-Longmaxi shale are indicated and derived from Hunt et al. (2012) and Liu et al. (2021a), respectively. Line correlation between $^{4}\text{He}^*/^{40}\text{Ar}^*$ and $^{1}/^{40}\text{Ar}^*$ ratios in the organic-rich shale (Dark gray solid line: $Y = 0.0001 \times + 16$, Fig. 9B) was established with the slope of ~ 0.0001 (purple fitting lines of Changning and Zheng'an samples suggest a slope of ~ 0.0001) and the minimum $^{4}\text{He}^*/^{40}\text{Ar}^*$ of ~ 15 . (For interpretation of the references to colour in this figure legend, the reader is referred to the web version of this article.)

the Wufeng-Longmaxi shale is slightly lower than the typical $^{40}\text{Ar}^*$ closure temperature (~ 230 – 300 °C) in K-bearing silicate minerals (Ballentine et al., 1994; Hunt et al., 2012; Snee, 2002), which will lead to an incomplete release of $^{40}\text{Ar}^*$ from the rock in the Wufeng-Longmaxi shale. Such incomplete Ar release would theoretically yield a

$^{4}\text{He}^*/^{40}\text{Ar}^*$ ratio higher than 15–17 or ~ 25 (Fig. 8B). However, the observed low $^{4}\text{He}^*/^{40}\text{Ar}^*$ ratio in the Wufeng-Longmaxi shale suggests an additional $^{40}\text{Ar}^*$ input or $^{4}\text{He}^*$ loss. If present, such external $^{40}\text{Ar}^*$ input is likely sourced from deeper crustal formations as mantle-derived noble gas is ruled out in the Wufeng-Longmaxi shale. Episodic $^{4}\text{He}^*$ loss, combined with incomplete release of $^{40}\text{Ar}^*$ in the Wufeng-Longmaxi shale, decreases the $^{4}\text{He}^*/^{40}\text{Ar}^*$ ratio in our gas samples (Fig. 8B). As illustrated in Fig. 8B, considering the situation of very little $^{40}\text{Ar}^*$ release at low temperature (i.e., i.e., high $^{1}/^{40}\text{Ar}^*$ value), two different initial $^{4}\text{He}^*/^{40}\text{Ar}^*$ ratios caused by episodic $^{4}\text{He}^*$ loss can be observed.

The Fuling and Zheng'an samples generally show $^{4}\text{He}^*/^{21}\text{Ne}^*$ ratios of $(1.06\text{--}1.64) \times 10^7$ and $(1.35\text{--}1.49) \times 10^7$, respectively (Table S3; Fig. 8C), which are lower than the measured $^{4}\text{He}^*/^{21}\text{Ne}^*$ ratio of the Changning field [$(1.93\text{--}3.05) \times 10^7$]. The Wufeng-Longmaxi shale is highly matured, corresponding to a maximum temperature of ~ 200 °C (at maximum burial depth), at which $^{4}\text{He}^*$ and $^{21}\text{Ne}^*$ would have been fully released. As the maturity of shale increases with reservoir temperature increasing, more $^{21}\text{Ne}^*$ will be released into pore fluids which will decrease the $^{4}\text{He}^*/^{21}\text{Ne}^*$ ratio in pore fluids. Relatively higher $^{4}\text{He}^*/^{21}\text{Ne}^*$ ratios of Changning samples than the Fuling and Zheng'an fields thus suggest a relatively higher proportion of pore fluid generated at low thermal maturity that is characterized by a higher $^{4}\text{He}^*/^{21}\text{Ne}^*$ ratio (Fig. 8C). In other words, the $^{4}\text{He}^*$ loss from the Paleozoic Wufeng-Longmaxi shale might occur much earlier (shallower burial depth, lower reservoir temperature) in the Changning fields than that in Fuling and Zheng'an fields (Figs. 8C). This is supported by the low $V_{\text{oil}}/V_{\text{water}}$ ratio caused by oil leakage during Triassic exhumation in the Changning area (Table S5). In contrast, low $^{4}\text{He}^*/^{21}\text{Ne}^*$ ratio of Fuling and Zheng'an samples was coupled with the low $V_{\text{gas}}/V_{\text{oil}}$ ratios driven by gas leakage during the Jurassic thrust-fold deformation (Dong et al., 2015; He et al., 2018; Li et al., 2018) (Fig. 8C, Table S5).

5.5. Fluid retention time

Calculated Ne ages (estimated by Eq. 16 of Text S6) are ~ 28 to 2 Ma, ~ 177 to 99 Ma, and ~ 250 to 24 Ma for Fuling, Zheng'an, and Changning samples, respectively (Table S3, Fig. 2C). The very young Ne age of Fuling samples suggests that the accumulation of nucleogenic $^{21}\text{Ne}^*$ (and so the mixing of two Ne endmembers) might not initiate until the onset of Jurassic thrust-fold deformation (particularly, the Late Eocene Qiyueshan Uplift (Feng et al., 2023)) (Fig. 2C). This is also consistent with the low $C_1/^{36}\text{Ar}$ ratios caused by more fluids leakage. Due to the similar solubility of C_1 and Ar in water, no significant solubility-driven fractionation will occur between C_1 and Ar during the mixing and gas-water phases separating (Ballentine et al., 1991). Measured $C_1/^{36}\text{Ar}$ ratios of Fuling gas samples generally align with the predicted ratios for a gas phase stripping ASW under the current reservoir conditions (Fig. 9), indicating that both methane and noble gas in the Wufeng-Longmaxi shale of Fuling field were primarily governed by gas stripping of present formation water. Before the gas stripping, most of free-phase gas may have been expelled from the Wufeng-Longmaxi shale of Fuling field due to the trigger of fault activation, considering that the special tectonic location of Fuling field that is located in the vicinity of the Qiyueshan Fault (the eastern boundary of Sichuan Basin) and the Qiyueshan Fault was significantly uplifted during Late Eocene (Feng et al., 2023; Liu et al., 2020a) (Fig. 1B). Unlike Fuling, $C_1/^{36}\text{Ar}$ ratios of Zheng'an and Changning samples are generally greater than the predicted values assuming present reservoir depths, suggesting a better preservation of early-generated natural gas during tectonic exhumation (Fig. 9). The Ne age confirms that, the binary mixing of End-members 1 and 2 in the Wufeng-Longmaxi shale of the Zheng'an field, occurred slightly before the onset of Jurassic deformation, and aligned the transition from oil window to gas window as indicated thermal maturity of $>1.3\% \text{Ro}$ (vitrinite reflectance) at ~ 177 Ma (Fig. 2C). Despite the wide range of Ne age may imply the heterogeneity in fluid retention time, the maximum Ne age roughly aligned with the Triassic deformation of the

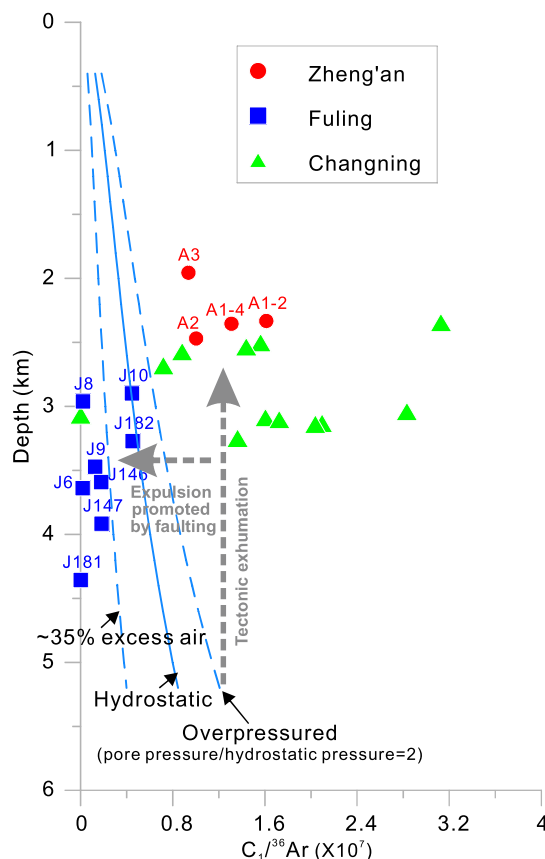


Fig. 9. Measured ratios of methane (C_1) to ^{36}Ar in the Upper Yangtze Block as a function of depth. These are compared with the $C_1/^{36}\text{Ar}$ ratio expected for a C_1 saturated and air-saturated seawater ($25\text{ }^\circ\text{C}$, 5 M NaCl) at the reservoir temperature [geothermal gradient = $23\text{ }^\circ\text{C/km}$ (Liu et al., 2021a)] and pressure (hydrostatic and overpressure).

Wufeng-Longmaxi shale Changning filed (Fig. 2C). In other words, the binary mixing of Endmembers 3 and 2 in the Wufeng-Longmaxi shale of the Changning filed, primarily began after the Triassic deformation (Fig. 2C).

A general timeline in the Wufeng-Longmaxi shale of the Upper Yangtze block is thus summarized here (Fig. 10): 1) the onset of the Triassic exhumation of the western Yangtze Block induced the oil leakage in the Changning field, the oil leakage decreased $V_{\text{oil}}/V_{\text{water}}$

ratio (Table S5) and inhibited the solubility fractionation during the oil-water interaction in the shale pore system (Fig. 7B), meanwhile, the oil leakage was also accompanied by a early ^4He loss (at low thermal maturity) which decreased $^4\text{He}*/^{40}\text{Ar}^*$ ratio (Fig. 8A, B); 2) the Jurassic thrust-fold deformation of the central Yangtze Block induced the gas leakage in the Fuling and Zheng'an fields, the gas leakage decreased $V_{\text{gas}}/V_{\text{oil}}$ ratio in the shale pore system (Table S5) and was accompanied by a late ^4He loss (at high thermal maturity) which decreased both $^4\text{He}*/^{40}\text{Ar}^*$ and $^4\text{He}*/^{21}\text{Ne}^*$ ratios almost at the maximum burial depth (Figs. 2C, 8B, C); 3) the massive expulsion of natural gas decreased the $C_1/^{36}\text{Ar}$ ratios of the Fuling samples because of activation of the Qiyueshan Fault during exhumation (Feng et al., 2023) (Figs. 2C, 9).

6. Conclusions

Shale gas samples, collected from the Fuling and Zheng'an gas fields that target the Paleozoic Wufeng-Longmaxi shale in the Upper Yangtze Block, are analyzed for noble gas and hydrocarbon compositions and presented together with previous data obtained from the Changning field – targeting the same shale – for sake of comparison.

Gas samples generally present higher $\delta^{13}\text{C}-C_1$ values than $\delta^{13}\text{C}-C_2$ suggesting hydrocarbon gases are generated by the secondary cracking of retained oil (or wet gas) at elevated maturity. Noble gases are dominated by atmosphere- and crust-derived sources. Atmospheric noble gas elemental ratios (e.g., $^{20}\text{Ne}_{\text{air-frac}}/^{36}\text{Ar}$ and $^{84}\text{Kr}/^{36}\text{Ar}$) record the temporal and spatial variation in the relative volume of oil, water, and gas phases in the Upper Yangtze Block. Highly fractionated $^{20}\text{Ne}_{\text{air-frac}}/^{36}\text{Ar}$ and $^{84}\text{Kr}/^{36}\text{Ar}$ ratios are best explained by multi-phase interactions involving oil, water, and gas phases over geologic time. In particular, more oil-phase is likely expelled in the Triassic forebulge of the western Yangtze Block, as indicated by the low $V_{\text{oil}}/V_{\text{water}}$ ratio during the water-oil phases fractionation in the Changning field. In contrast, a more extensive gas expulsion in the Jurassic thrust-fold belts of the central-eastern Yangtze Block can be revealed by the abnormally low $V_{\text{gas}}/V_{\text{oil}}$ ratio after the water-gas phases fractionation in the Fuling and Zheng'an fields. A study of crustal noble gas composition in our gas samples sheds light on the temporal and spatial variation in the fluid leakage from the Wufeng-Longmaxi shale of the Upper Yangtze Block. Calculated radiogenic ^4He of our gas samples are generally several orders lower than the predicted accumulated $^4\text{He}^*$ assuming ^4He is solely produced in-situ by U and Th contents within the Wufeng-Longmaxi shale. This likely points to episodic ^4He loss from the Wufeng-Longmaxi shale. The range of $^4\text{He}^*/^{21}\text{Ne}^*$ ratios varies from field to field in the Wufeng-Longmaxi shale. We propose that this might be best explained by that ^4He loss occurred earlier in the Changning field than

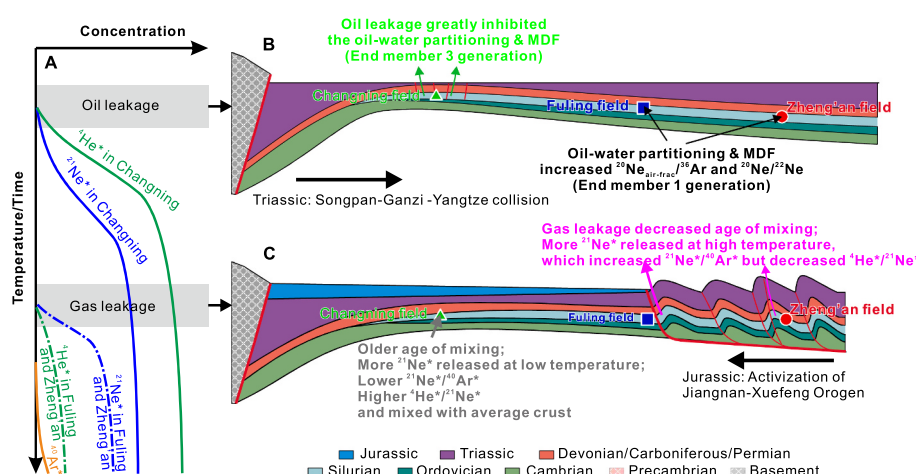


Fig. 10. Schematic illustration showing the spatial-temporal variation in noble gas signatures in the Wufeng-Longmaxi shale of the Upper Yangtze Block. There were two episodes of He loss (A) caused by the Triassic (B) and Jurassic-Cretaceous (C) tectonic deformations.

the Fuling and Zheng'an fields, which is consistent with the Triassic exhumation of the western Yangtze Block and the Jurassic fold-thrust deformation of the central-eastern Yangtze Block.

CRediT authorship contribution statement

Rui Liu: Writing – review & editing, Writing – original draft, Visualization, Investigation, Data curation. **Tao Wen:** Writing – review & editing, Writing – original draft, Investigation. **Daniele L. Pinti:** Writing – review & editing, Investigation. **Rui Xu:** Writing – review & editing. **Fang Hao:** Writing – review & editing. **Shang Xu:** Writing – review & editing. **Zhiguo Shu:** Writing – review & editing.

Declaration of competing interest

The authors declare that they have no known competing financial interests or personal relationships that could have appeared to influence the work reported in this paper.

Data availability

All data discussed in this manuscript has been included in tables. These datasets are also made available under the MIT license via this Zenodo data DOI: <https://doi.org/10.5281/zenodo.6963862>.

Acknowledgments

This research was supported by the National Natural Science Foundation of China (No. 42072184, 41702157) and the Science and Technology Cooperation Project of the CNPC-SWPU Innovation Alliance (2020CX010302).

Appendix A. Supplementary data

Supplementary data to this article can be found online at <https://doi.org/10.1016/j.coal.2024.104671>.

References

- Ballentine, C.J., Burnard, P.G., 2002. Production, Release and Transport of Noble gases in the Continental Crust. *Rev. Mineral. Geochem.* 47 (1), 481–538.
- Ballentine, C.J., O'Nions, R.K., 1992. The nature of mantle neon contributions to Vienna Basin hydrocarbon reservoirs. *Earth Planet. Sci. Lett.* 113 (4), 553–567.
- Ballentine, C.J., O'Nions, R.K., Oxburgh, E.R., Horvath, F., Deak, J., 1991. Rare gas constraints on hydrocarbon accumulation, crustal degassing and groundwater flow in the Pannonian Basin. *Earth Planet. Sci. Lett.* 105 (1), 229–246.
- Ballentine, C.J., Mazurek, M., Gautschi, A., 1994. Thermal constraints on crustal rare gas release and migration: evidence from Alpine fluid inclusions. *Geochim. Cosmochim. Acta* 58 (20), 4333–4348.
- Ballentine, C.J., Burgess, R., Marty, B., 2002. Tracing Fluid Origin, Transport and Interaction in the Crust. *Rev. Mineral. Geochem.* 47 (1), 539–614.
- Bosch, A., Mazor, E., 1988. Natural gas association with water and oil as depicted by atmospheric noble gases: case studies from the southeastern Mediterranean Coastal Plain. *Earth Planet. Sci. Lett.* 87 (3), 338–346.
- Buttitta, D., et al., 2020. Continental degassing of helium in an active tectonic setting (northern Italy): the role of seismicity. *Sci. Rep.* 10 (1), 162.
- Byrne, D.J., Barry, P.H., Lawson, M., Ballentine, C.J., 2018. Determining gas expulsion vs retention during hydrocarbon generation in the Eagle Ford Shale using noble gases. *Geochim. Cosmochim. Acta* 241, 240–254.
- Byrne, D.J., Barry, P.H., Lawson, M., Ballentine, C.J., 2020. The use of noble gas isotopes to constrain subsurface fluid flow and hydrocarbon migration in the East Texas Basin. *Geochim. Cosmochim. Acta* 268, 186–208.
- Castro, M.C., Ma, L., Hall, C.M., 2009. A primordial, solar He–Ne signature in crustal fluids of a stable continental region. *Earth Planet. Sci. Lett.* 279 (3), 174–184.
- Cheng, A., et al., 2021. Determining the role of diffusion and basement flux in controlling ^4He distribution in sedimentary basin fluids. *Earth Planet. Sci. Lett.* 574, 117175.
- Cheng, A., Sherwood Lollar, B., Gluyas, J.G., Ballentine, C.J., 2023. Primary N₂-He gas field formation in intracratonic sedimentary basins. *Nature* 615 (7950), 94–99.
- Clarke, W.B., Jenkins, W.J., Top, Z., 1976. Determination of tritium by mass spectrometric measurement of ^3He . *Int. J. Appl. Radiat. Isot.* 27 (9), 515–522.
- Craig, H., 1957. Isotopic standards for carbon and oxygen and correction factors for mass-spectrometric analysis of carbon dioxide. *Geochim. Cosmochim. Acta* 12 (1), 133–149.
- Dai, J., et al., 2016. Geochemical characteristics of marine and terrestrial shale gas in China. *Mar. Pet. Geol.* 76, 444–463.
- Darrah, T.H., Vengosh, A., Jackson, R.B., Warner, N.R., Poreda, R.J., 2014. Noble gases identify the mechanisms of fugitive gas contamination in drinking-water wells overlying the Marcellus and Barnett Shales. In: *Proceedings of the National Academy of Sciences*, p. 201322107.
- Dong, S.W., et al., 2015. A possible buried Paleoproterozoic collisional orogen beneath central South China: evidence from seismic-reflection profiling. *Precambrian Res.* 264, 1–10.
- Eberhardt, P., Eugster, O., Marti, K., 1965. Notizen: a Redetermination of the Isotopic Composition of Atmospheric Neon. *Zeitschrift für Naturforschung A* 20 (4), 623–624.
- Feng, Z., et al., 2022. Shale gas geochemistry in the Sichuan Basin, China. *Earth-Sci. Rev.* 232, 104141.
- Feng, Q., et al., 2023. Effect of tectonic reworking on shale fracturing and gas preservation in the upper Yangtze block, South China. *Mar. Pet. Geol.* 148, 106069.
- Gao, J., He, S., Zhao, J.-x., Yi, J., 2017. Geothermometry and geobarometry of overpressured lower Paleozoic gas shales in the Jiaoshiba field, Central China: Insight from fluid inclusions in fracture cements. *Mar. Pet. Geol.*, 83: 124–139.
- Gilliland, S.M.V., et al., 2008. The noble gas geochemistry of natural CO₂ gas reservoirs from the Colorado Plateau and Rocky Mountain provinces, USA. *Geochim. Cosmochim. Acta* 72 (4), 1174–1198.
- Graham, D.W., 2002. Noble Gas Isotope Geochemistry of Mid-Ocean Ridge and Ocean Island Basalts: Characterization of Mantle Source Reservoirs. *Rev. Mineral. Geochim.* 47 (1), 247–317.
- Györe, D., Tait, A., Hamilton, D., Stuart, F.M., 2019. The formation of NeH⁺ in static vacuum mass spectrometers and re-determination of 21Ne/20Ne of air. *Geochim. Cosmochim. Acta* 263, 1–12.
- Györe, D., Pujol, M., Gilfillan, S.M.V., Stuart, F.M., 2021. Noble gases constrain the origin, age and fate of CO₂ in the Vaca Muerta Shale in the Neuquén Basin (Argentina). *Chem. Geol.* 577, 120294.
- Györe, D., et al., 2024. Inter-laboratory re-determination of the atmospheric 22Ne/20Ne. *Chem. Geol.* 645, 121900.
- Hao, F., Zou, H., 2013. Cause of shale gas geochemical anomalies and mechanisms for gas enrichment and depletion in high-maturity shales. *Mar. Pet. Geol.* 44, 1–12.
- He, W., Zhou, J., Yuan, K., 2018. Deformation evolution of Eastern Sichuan–Xuefeng fold-thrust belt in South China: Insights from analogue modelling. *J. Struct. Geol.* 109, 74–85.
- Hunt, A.G., Darrah, T.H., Poreda, R.J., 2012. Determining the source and genetic fingerprint of natural gases using noble gas geochemistry: a northern Appalachian Basin case study. *AAPG Bull.* 96 (10), 1785–1811.
- Kennedy, B.M., Soest, M.C.v., 2007. Flow of Mantle Fluids through the Ductile lower Crust: Helium Isotope Trends. *Science* 318 (5855), 1433–1436.
- Kennedy, B.M., Torgersen, T., van Soest, M.C., 2002. Multiple atmospheric noble gas components in hydrocarbon reservoirs: a study of the Northwest Shelf, Delaware Basin, SE New Mexico. *Geochim. Cosmochim. Acta* 66 (16), 2807–2822.
- Kharaka, Y.K., Specht, D.J., 1988. The solubility of noble gases in crude oil at 25–100°C. *Appl. Geochem.* 3 (2), 137–144.
- Lee, J.-Y., et al., 2006. A redetermination of the isotopic abundances of atmospheric Ar. *Geochim. Cosmochim. Acta* 70 (17), 4507–4512.
- Li, J., et al., 2018. An Andean-type retro-arc foreland system beneath northwest South China revealed by SINOPROBE profiling. *Earth Planet. Sci. Lett.* 490, 170–179.
- Liu, R., et al., 2020a. Influence of tectonic exhumation on porosity of Wufeng–Longmaxi shale in the Fuling gas field of the eastern Sichuan Basin, China. *AAPG Bull.* 104 (4), 939–959.
- Liu, R., et al., 2020b. Variation in pore systems with tectonic stress in the overthrust Wufeng–Longmaxi shale of the southern Sichuan Basin, China. *J. Nat. Gas Sci. Eng.* 83, 103617.
- Liu, W., et al., 2020c. Hydrocarbon generation and shale gas accumulation in the Wufeng–Longmaxi formations, Changning shale-gas field, Southern Sichuan Basin. *J. Nanjing Univ. (Natural Science)* 56, 393–404.
- Liu, R., et al., 2021a. The dichotomy in noble gas signatures linked to tectonic deformation in Wufeng–Longmaxi Shale, Sichuan Basin. *Chem. Geol.* 581, 120412.
- Liu, S., et al., 2021b. Tectonic evolution of the Sichuan Basin, Southwest China. *Earth Sci. Rev.* 213, 103470.
- Liu, W., et al., 2021c. Cenozoic exhumation and shale-gas enrichment of the Wufeng–Longmaxi formation in the southern Sichuan basin, western China. *Mar. Pet. Geol.* 125, 104865.
- Lorant, F., Prinzhofner, A., Behar, F., Huc, A.-Y., 1998. Carbon isotopic and molecular constraints on the formation and the expulsion of thermogenic hydrocarbon gases. *Chem. Geol.* 147 (3), 249–264.
- Lowenstein, J.B., Evans, W.C., Bergfeld, D., Hunt, A.G., 2014. Prodigious degassing of a billion years of accumulated radiogenic helium at Yellowstone. *Nature* 506 (7488), 355–358.
- Mark, D.F., Stuart, F.M., de Podesta, M., 2011. New high-precision measurements of the isotopic composition of atmospheric argon. *Geochim. Cosmochim. Acta* 75 (23), 7494–7501.
- Méjean, P., Pinti, D.L., Ghaleb, B., Larocque, M., 2017. Fracturing-induced release of radiogenic ^4He and ^{234}U into groundwater during the last deglaciation: an alternative source to crustal helium fluxes in periglacial aquifers. *Water Resour. Res.* 53 (7), 5677–5689.
- Meng, Q.R., Wang, E., Hu, J.M., 2005. Mesozoic sedimentary evolution of the Northwest Sichuan basin: Implication for continued clockwise rotation of the South China block. *Geol. Soc. Am. Bull.* 117 (3–4), 396–410.

- Milkov, A.V., Faiz, M., Etiope, G., 2020. Geochemistry of shale gases from around the world: Composition, origins, isotope reversals and rollovers, and implications for the exploration of shale plays. *Org. Geochem.* 103997.
- Moore, M.T., et al., 2018. Differentiating between Biogenic and Thermogenic Sources of Natural Gas in Coalbed Methane Reservoirs from the Illinois Basin Using Noble Gas and Hydrocarbon Geochemistry, From Source to Seep: Geochemical Applications in Hydrocarbon Systems. Geological Society of London, pp. 0.
- Mtini, K.M., et al., 2021. The origin of high helium concentrations in the gas fields of southwestern Tanzania. *Chem. Geol.* 585, 120542.
- Oxburgh, E.R., O'Nions, R.K., Hill, R.I., 1986. Helium isotopes in sedimentary basins. *Nature* 324 (6098), 632–635.
- Ozima, M., Podosek, F.A., 2002. Noble gas Geochemistry. Cambridge University Press, New York.
- Pearson, D.G., et al., 2021. Deep continental roots and cratons. *Nature* 596 (7871), 199–210.
- Pinti, D.L., Marty, B., 1995. Noble gases in crude oils from the Paris Basin, France: Implications for the origin of fluids and constraints on oil-water-gas interactions. *Geochim. Cosmochim. Acta* 59 (16), 3389–3404.
- Pinti, D.L., et al., 2011. Fossil brines preserved in the St-Lawrence Lowlands, Québec, Canada as revealed by their chemistry and noble gas isotopes. *Geochim. Cosmochim. Acta* 75 (15), 4228–4243.
- Pinti, D.L., Castro, M.C., Lopez-Hernandez, A., Han, G., Shouakar-Stash, O., Hall, C.M., Ramírez-Montes, M., 2017. Fluid circulation and reservoir conditions of the Los Humeros Geothermal Field (LHGF), Mexico, as revealed by a noble gas survey. *J. Volcanol. Geotherm. Res.* <https://doi.org/10.1016/j.jvolgeores.2017.01.015>.
- Prinzhofer, A.A., Huc, A.Y., 1995. Genetic and post-genetic molecular and isotopic fractionations in natural gases. *Chem. Geol.* 126 (3), 281–290.
- Richardson, N.J., et al., 2008. Extraordinary denudation in the Sichuan Basin: Insights from low-temperature thermochronology adjacent to the eastern margin of the Tibetan Plateau. *J. Geophys. Res. Solid Earth* 113 (B4), 23.
- Smith, S.P., Kennedy, B.M., 1983. The solubility of noble gases in water and in NaCl brine. *Geochim. Cosmochim. Acta* 47 (3), 503–515.
- Snee, L.W., 2002. Argon Thermochronology of Mineral Deposits; a Review of Analytical Methods, Formulations, and Selected Applications (USGS).
- Wang, L., Griffin, W.L., Yu, J., O'Reilly, S.Y., 2010. Precambrian crustal evolution of the Yangtze Block tracked by detrital zircons from Neoproterozoic sedimentary rocks. *Precambrian Res.* 177 (1), 131–144.
- Wang, Y.J., Fan, W.M., Zhang, G.W., Zhang, Y.H., 2013. Phanerozoic tectonics of the South China Block: Key observations and controversies. *Gondwana Res.* 23 (4), 1273–1305.
- Weiss, R.F., 1971a. The effect of salinity on the solubility of argon in seawater. *Deep-Sea Res. Oceanogr. Abstr.* 18 (2), 225–230.
- Weiss, R.F., 1971b. Solubility of helium and neon in water and seawater. *J. Chem. Eng. Data* 16 (2), 235–241.
- Wen, T., Castro, M.C., Ellis, B.R., Hall, C.M., Lohmann, K.C., 2015. Assessing compositional variability and migration of natural gas in the Antrim Shale in the Michigan Basin using noble gas geochemistry. *Chem. Geol.* 417, 356–370.
- Wen, T., et al., 2016. Methane sources and Migration Mechanisms in Shallow Groundwaters in Parker and Hood Counties, Texas—a Heavy Noble Gas Analysis. *Environ. Sci. Technol.* 50 (21), 12012–12021.
- Wen, T., et al., 2017. Characterizing the Noble Gas Isotopic Composition of the Barnett Shale and Strawn Group and Constraining the source of Stray Gas in the Trinity Aquifer, North-Central Texas. *Environ. Sci. Technol.* 51 (11), 6533–6541.
- Wen, T., Pinti, D.L., Castro, M.C., López-Hernández, A., Hall, C.M., Shouakar-Stash, O., Sandoval-Medina, F., 2018. A noble gas and 87Sr/86Sr study in fluids of the Los Azufres geothermal field, Mexico – Assessing impact of exploitation and constraining heat sources. *Chem. Geol.* 483, 426–441. <https://doi.org/10.1016/j.chemgeo.2018.03.010>.
- Yang, R., He, S., Hu, Q., Hu, D., Yi, J., 2017. Geochemical characteristics and origin of natural gas from Wufeng-Longmaxi shales of the Fuling gas field, Sichuan Basin (China). *Int. J. Coal Geol.* 171, 1–11.
- Yang, G., et al., 2021. Hydrocarbon accumulation characteristics and enrichment laws of multi-layered reservoirs in the Sichuan Basin. *Nat. Gas Ind.* 36 (11), 1–11.
- Zaputlyeva, A., Mazzini, A., Caracausi, A., Sciarra, A., 2019. Mantle-Derived Fluids in the East Java Sedimentary Basin, Indonesia. *J. Geophys. Res. Solid Earth* 124 (8), 7962–7977.
- Zhai, G., et al., 2017. Peservoir-forming pattern of "four-storey" hydrocarbon accumulation in Anchang syncline of northern Guizhou Province. *Geol. China* 44 (1), 1–12 (in Chinese with English abstract).
- Zhou, Z., Ballentine, C.J., Schoell, M., Stevens, S.H., 2012. Identifying and quantifying natural CO₂ sequestration processes over geological timescales: the Jackson Dome CO₂ Deposit, USA. *Geochim. Cosmochim. Acta* 86, 257–275.
- Zou, C., et al., 2018. Ocean euxinia and climate change "double whammy" drove the late Ordovician mass extinction. *Geology* 46 (6), 535–538.
- Zou, C., et al., 2021. Development progress, potential and prospect of shale gas in China. *Nat. Gas Ind.* 41 (1), 1–14.